Journal of Soils and Sediments (2024) 24:259–274
https://doi.org/10.1007/s11368-023-03618-4

SOILS, SEC 4 • ECOTOXICOLOGY • RESEARCH ARTICLE

Enhanced immobilization of cadmium in contaminated paddy soil by biochar-supported sulfidized nanoscale zero-valent iron

Yiqun Xu[1] · Shan Cao[1] · Xinyu Chen[1] · Jun Li[1] · Hongdou Liu[1] · Yang Gao[2] · Siqi Wen[1] · Jiaming Guo[1] · Xiaoyu Shi[1] · Wenjing Xue[1]

Received: 30 March 2023 / Accepted: 22 July 2023 / Published online: 28 July 2023

Abstract

Purpose Nanoscale zero-valent iron (nZVI) is increasingly used to enhance the immobilization of cadmium (Cd) in paddy soil, but its application has limitations by various inherent disadvantages, such as easy passivation, agglomeration, and poor electron transfer. To overcome the drawback, biochar-supported sulfidized nZVI (S-nZVI/BC) was synthesized and added into Cd-contaminated paddy soil to investigate its immobilization performance and remediation mechanisms for Cd.

Materials and methods The synthesized materials were characterized by various techniques such as SEM, TEM, XPS, and FTIR. Sequential extraction method was adopted to examine the chemical speciation of Cd. The diethylenetriamine pentaacetic acid (DTPA)-extractable Cd and toxicity characteristic leaching procedure (TCLP)-leachable Cd were measured to evaluate the availability and leaching toxicity of Cd. The changes of soil properties and the reaction mechanism between Cd and S-nZVI/BC were also analyzed.

Results and discussion Sequential extraction procedure suggested that S-nZVI/BC was effective in transforming mobile Cd to stable speciation with the proportion of residual speciation increased by 32.04% after 49 days of treatment. The DTPA-extractable Cd content decreased from 2.14 to 0.42 mg·kg^{-1}, indicating the availability of Cd was significantly reduced. Meanwhile, the immobilization efficiency of TCLP-leachable Cd was increased by 53.70%, showing that S-nZVI/BC reduced the leaching toxicity and environmental risk of Cd. Also, it was found that the addition of S-nZVI/BC increased the soil pH, redox potential (Eh), and organic matter (OM), of which pH was the main factor influencing soil Cd mobility. Furthermore, characterization results of S-nZVI/BC after remediation clarified that the stabilization mechanism of Cd was mainly dominated by the adsorption, complexation, and precipitation of Cd^{2+} with BC and the iron oxide/hydroxide or FeS_x shell of S-nZVI and secondary iron minerals ($CdFe_2O_4$).

Conclusion Overall, S-nZVI/BC could be an effective material for the remediation of Cd-contaminated soil and alleviate the hazards likely posed to the environment. This work offers a new avenue for practical applications of nZVI-based materials in contamination remediation.

Keywords Cadmium · Paddy soil · Immobilization effect · Sulfidized nanoscale zero-valent iron · Biochar

1 Introduction

In the agricultural environment, cadmium (Cd) is one of the most hazardous heavy metals (Xiao et al. 2023). Cd contamination in paddy soil is a growing concern because it poses a serious threat to global food security and public health (Liu et al. 2021; Wang et al. 2022). According to the national survey bulletin of soil contamination in 2014, approximately 19.4% of China's agricultural soil contains organic contaminants or inorganic heavy metals exceeding the standard, in which the over-standard rate of soil Cd contamination was 7.0% (Huang et al. 2021). Therefore, an urgently effective

Responsible editor: Dong-Mei Zhou

✉ Wenjing Xue
xuewenjing@yzu.edu.cn

[1] College of Environmental Science and Engineering, Yangzhou University, Yangzhou 225009, People's Republic of China

[2] School of Hydraulic and Environmental Engineering, Changsha University of Science & Technology, Changsha 410114, People's Republic of China

strategy is required to address the risks of Cd contamination to the safety of rice.

With the advancements of nanotechnology, iron-based nanomaterials have been extensively utilized to treat Cd-contaminated paddy soil (Yang et al. 2021a). Among them, nanoscale zero-valent iron (nZVI) has garnered the most interest owing to its unique nano core–shell structure, and its application potential for efficient stabilization of heavy metals (Yang et al. 2021a). Nevertheless, there are also some inherent defects in nZVI, such as easy passivation, aggregation, and poor electron selectivity (Liu et al. 2022). To overcome these limitations, some modifications of nZVI have been proposed, including loading (Jin et al. 2023), bimetallic (Dong et al. 2022), surface coating (Zhang et al. 2022b), and sulfidation (Liang et al. 2021b). Especially, sulfidized nZVI (S-nZVI) is considered an excellent modification method and gained intensive research in recent years (Liang et al. 2021b; Yuan et al. 2022). FeS_x layer generated from S-nZVI not only inhibits the oxidation of nZVI and prolongs its reactive lifetime, but also promotes the transfer of electrons from the Fe^0 core to the surface layer and enhances the reaction ability of nZVI (Yuan et al. 2022). Moreover, FeS_x can immobilize heavy metals by adsorption, co-precipitation, ion exchange, etc. (Gao et al. 2022b). However, S-nZVI particles still easily agglomerate due to their hydrophobicity, magnetic, and nano properties (Gao et al. 2022a). As a porous structure carbonaceous solid, biochar (BC) is commonly used as a supporting material for iron-based nanomaterials (Yang et al. 2021a). In addition, BC has been regarded as a green and effective remediation agent for soil heavy due to its unique properties, such as high surface area, abundant pore structures, terrific amount of functional groups, and huge cation exchange capacity (Ma et al. 2022a). Therefore, it is expected that loading S-nZVI on BC supported not only increase the dispersion of S-nZVI and enhance its immobilization to Cd. The application of S-nZVI/BC nanomaterials for the Cd remediation of contaminated paddy soil is still uncommon, despite some experimental researches on the reduction of heavy metal pollution or the degradation of organic pollution (Gao et al. 2022a, b).

A successful immobilization technology is closely related to the migration and transformation capacity of contaminants in environmental media (Ma et al. 2022a; Yang et al. 2021a). The more active heavy metals speciation, such as the acid soluble speciation, which exhibited high mobility and bioavailability, was typically more likely to be altered in the environment. In contrast, the stability phase (residual speciation) was less mobile and higher safety, with a lower environmental risk (Jin et al. 2023). Hence, the modified Community Bureau of Reference (BCR) sequential extraction method was adopted to examine variations in Cd chemical speciation. Besides, the metals availability and leaching toxicity to be tested in the soil can be considered as comprehensive indicators to evaluate the biological effects of heavy metals during the remediation process, which has significant scientific value for comprehending how S-nZVI/BC reduces the potential ecological risks of heavy metal during the remediation of contaminated soil (Jiang et al. 2022a). Furthermore, the surface charge of soil colloids or nanomaterials can change depending on the pH of the soil, which is a critical element in controlling the tendency of heavy metals to migrate (Liu et al. 2022; Wang et al. 2021b). Notably, soil redox potential (Eh) was important to the mobility of heavy metals, the decrease of Eh was contributed to the generation of insoluble heavy metal compounds (Yang et al. 2021a). Also, previous researches have found that soil organic matter (OM) may influence the chemical behaviors of heavy metals such as sorption–resolution, complexation, and solution–precipitation (Fan et al. 2023). However, valid information about S-nZVI/BC caused alterations in soil pH and OM and the influence of pH and OM changes on Cd immobilization are still unclear, and further researches are necessary.

The research goals are listed as follows: (i) synthesize and characterize S-nZVI/BC nanomaterials; (ii) explore the effect of S-nZVI/BC on Cd immobilization by detecting the change of Cd speciation in contaminated paddy soils; (iii) evaluate the ecological risk of S-nZVI/BC by measuring the availability and leaching toxicity of Cd; (iv) analyze the possible interaction mechanisms between the S-nZVI/BC and Cd by further determining soil pH, Eh, OM, and S-nZVI/BC. The theoretical underpinnings for the efficient application of S-nZVI/BC in the treatment of Cd-contaminated paddy soil are provided by this work.

2 Materials and methods

2.1 Chemical reagents and soil properties

The wheat straw was purchased from Yangzhou Yang-Tai Medical Instrument Co., Ltd (Jiangsu, China). Iron trichloride hexahydrate ($FeCl_3{\cdot}6H_2O$, 99.0%), sodium borohydride ($NaBH_4$, 98.0%), sodium dithionite ($Na_2S_2O_4$, 99.0%), hydrogen nitrate (HNO_3), and absolute alcohol (C_2H_5OH) were obtained from Sinopharm Chemical Reagent Co., Ltd (Shanghai, China). Chemicals of analytical grade were employed without additional purification throughout the experiment. To prepare all solutions, ultrapure water (18.2 MΩ·cm) was utilized. Trial soil was provided from the surface soil (0–20 cm) of a paddy field in Hanjiang, Yangzhou, Jiangsu Province, China. Supporting Information (SI) provided specifics regarding the soil collection and subsequent treatment.

2.2 Synthesis and characterization of nanomaterials

BC was prepared according to the method provided by modified Gao et al. (2022a). Specifically, BC was derived pyrolysis of crushed wheat straw placed in a quartz boat in a tubular furnace with a nitrogen-filled environment. The pyrolysis process was elevated to 600 °C at 5 °C·min^{-1} and then maintained the temperature under nitrogen protection for 2 h. Finally, ground the solid into powder after cooling to room temperature, and collected after passing through a 0.15-mm sieve to obtain the desired BC.

S-nZVI/BC was synthesized by using $NaBH_4$ as the reducing agent to reduce Fe^{3+} solution (Jiang et al. 2022b). Firstly, after transferring 100 mL of 2.4152 g $FeCl_3{\cdot}6H_2O$ solution to a three-necked flask and adding 1.0 g of BC to the flask, the mixed solution was stirred for 30 min under a flow of nitrogen to remove the residual air in the solution. Secondly, 1.6 g of $NaBH_4$ and 0.1942 g of $Na_2S_2O_4$ were prepared as a 100-mL mixed solution, and the solution was added dropwise to the continuously stirred solution in the three-necked flask, then after dropping, continue stirring for 30 min to full reaction. Subsequently, a magnet was used to separate solids and liquids in the reaction solution, then discarded the supernatant, washed the remaining black precipitates with ethanol three times to remove impurities, and the black precipitates were dried in a vacuum drying box for 8 h (60 °C) to obtain the S-nZVI/BC. Finally, S-nZVI/BC was ground and stored for later use. The preparation flow chart of the S-nZVI/BC was depicted in Fig. 1. The preparation procedure of nZVI, nZVI/BC, and S-nZVI were similar to that described above, nZVI was synthesized without adding BC and $Na_2S_2O_4$, nZVI/BC was attained without adding $Na_2S_2O_4$, and S-nZVI was obtained without adding BC. The pH of the nanomaterials and the characterization details of the nanomaterials before and after the reaction were shown in the SI.

2.3 Experiment design

For paddy soil remediation, the appropriate amount of stored dry paddy soil was placed in a 50-mL-circled plastic centrifuge tube, then the nanomaterials were incorporated into the soil at a ratio of 0.03:1 mass of nanomaterials to soil, and all the samples were shaken uniformly and mix thoroughly. Then, an appropriate amount of ultrapure water was added to simulate the state of a paddy field during flooding, and the soil-to-water ratio was 1:5. The control group experiment was conducted without any nanomaterial and the circumstances for the experiments were unchanged. The soil samples were assayed at 1, 7, 14, 21, 35, and 49 days in order to specifically examine how reaction time affects Cd immobilization. During the treatment period, each treatment group was cultured at room temperature, and its water holding capacity was continuously maintained by adding ultrapure water. After reaching the set treatment time, the paddy soil samples were centrifuged for further analysis.

2.4 Determination of Cd speciations, availability, and leachability

The Cd speciation in contaminated soil was identified by the BCR continuous extraction method proposed by Liu et al. (2018). Acid soluble, reducible, oxidizable, and residual are the four speciations of Cd that exist in soil. Usually, 0.11 M CH_3COOH and 0.5 M $NH_2OH{\cdot}HCl$ were used to extract the acid soluble and reducible, respectively. The oxidizable was extracted using H_2O_2 and 1 M NH_4OAc. The residual was digested with HNO_3-HF-$HClO_4$ (5: 4: 2) system. The soil Cd availability was assessed using the DTPA extraction method

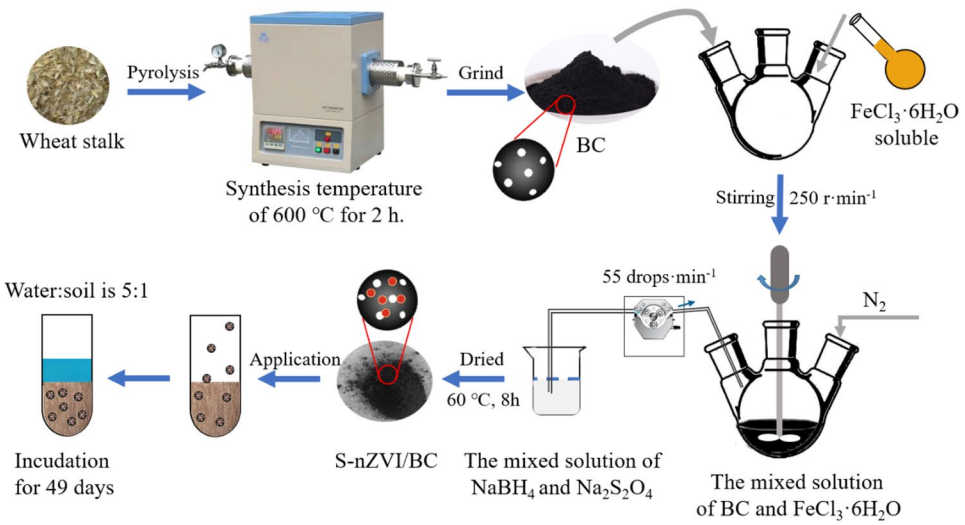

Fig. 1 Flow chart for the preparation of S-nZVI/BC nanomaterial

(Yang et al. 2021c). The TCLP test assessed Cd leachability (Liu et al. 2018). More details about the extraction steps were displayed in SI and Table S1.

2.5 pH, Eh, and OM measurement

A pH meter was employed to measure soil pH at the soil-to-water ratio of 1:5 (Puissant et al. 2019). The soil Eh value was measured and recorded by inserting compounding electrode in the soil. To clarify the contents of soil OM, the $K_2Cr_2O_7$ volumetric method was employed and the content of OM was obtained based on (Wang et al. 2021b):

$$\mathrm{OM}=\left[\frac{0.5\times(V_0-V)\times0.001\times3.0\times1.33}{m}\right]\times1000\times1.725 \quad (1)$$

where V_0 is the $FeSO_4$ consumption of the blank, V is the $FeSO_4$ consumption of the sample, and m is the weight of the soil.

2.6 Date process and statistical analyses

All experiments in this study were conducted three times and all outcomes were expressed as mean values ± standard deviation and drawn with Origin 2018 software (Northampton, MA, USA). Version 26.0 of the IBM SPSS Statistics for Windows (Armonk, NY, USA) was used for one-way analysis of variance (ANOVA) and Pearson correlation analysis.

3 Results and discussion

3.1 Characterization

The morphologies of nZVI, BC, S-nZVI, S-nZVI/BC by the scanning electron microscope (SEM) images were displayed in Fig. 2. The pristine nZVI particles were spherical and agglomerated together due to magnetic effect (Fig. 2a). From Fig. 2b, BC contained abundant pore structures, which could effectively disperse S-nZVI and provide more adsorption sites for heavy metals. S-nZVI particles displayed a rougher surface than nZVI, owing to the formation of an outer layer that contains a large amount of iron sulfide and a small amount of iron oxide (Fig. 2c) (Bhattacharjee and Ghoshal 2018; Han et al. 2019). Also, according to Fig. 2d, S-nZVI particles adhered to BC surfaces and displayed effective dispersion. The transmission electron microscopy (TEM) images suggested that the nZVI particles presented chain-like structure with size of about 50 nm (Fig. 2e). The TEM images of S-nZVI/BC revealed a sphere particle phase, where particles were remarkably dispersed (Fig. 2f). Significantly, BC was observed in the vicinity of the sphere particles.

The X-ray photoelectron spectroscopy (XPS) spectrum of S-nZVI/BC was presented in Fig. 3. During the survey spectrum analysis (Fig. 3a), the coexistence of Fe, C, O, and S elements was observed in S-nZVI/BC. Fe 2p3/2 and Fe 2p1/2 were visible at Fe 2p spectrum peaks in Fig. 3b, where the characteristic peaks at 708.9 eV and 719.7 eV were considered as the Fe^0 (Wang et al. 2021a), 710.1 eV and 724.5 eV were represented to the Fe^{2+} (Wang et al. 2021a), 713.0 eV and 731.2 eV were indicated the peaks of Fe^{3+} (Rao et al. 2021). The peak areas of 24.0%, 49.4%, and 26.6% for Fe^0, Fe^{2+}, and Fe^{3+}, respectively, demonstrate that Fe^{2+} was the dominant iron species in the nanomaterial. Peaks situated at 169.2, 167.8, 163.9, 162.9, 162.4, and 160.9 eV were ascribed to the S compounds (SO_4^{2-}, SO_3^{2-}, S_n^{2-}, S_2^{2-} and S^{2-}) with corresponding peak areas of 14.9%, 22.2%, 15.5%, 22.6%, and 24.8%, respectively (Fig. 3c) (Luo et al. 2022; Singh et al. 2021). The creation of a FeS_x-dominated layer was indicated by the detection of S^{2-}, S_2^{2-}, and S_n^{2-} species, which may have increased the reactivity of nanomaterial (Gao et al. 2022b). Also, the presence of SO_3^{2-} and SO_4^{2-} species suggested that some of the S were oxidized to form sulfur oxides during the synthesis process (Gao et al. 2022a). As depicted in Fig. 3d, it was determined that –COOH, C=O, C–O, and C=C were responsible for peaks at 293.5, 288.8, 284.4, and 283.9 eV of C1s (Fan et al. 2021; Wang et al. 2021a), respectively. Figure 3e displayed the peaks of O 1s at 532.2, 531.1, and 530.4 eV, considered as C=O, C–O, and -OH of BC (Khan et al. 2021; Luo et al. 2019), respectively. While the peak at 531.8 and 529.5 eV were corresponded to the presence of FeOOH and Fe–O in the nanomaterial (Hu et al. 2021; Zhu et al. 2020).

The Fourier transform infrared spectroscopy (FTIR) spectra of nZVI, BC, S-nZVI, nZVI/BC, and S-nZVI/BC were shown in Fig. 3f. The –OH bending vibration at 1404 cm^{-1} was observed in nZVI, which might be the hydroxylation reaction on nZVI surface (Tang et al. 2021). The bands at about 3500 cm^{-1} and 3700 cm^{-1} were explained by fluctuations in the O–H bonding of adsorbed water or the hydroxyl groups (–OH) stretching on the BC surface (Tang et al. 2021). In addition, the C=O stretch at 1667 cm^{-1} (Luo et al. 2019), the $-CH_2$ stretch at 1470 cm^{-1} (Huang et al. 2020) and the –OH bending vibration at 1265 cm^{-1} were assigned to BC (Liu et al. 2018). The stretching vibrations of C–O and C–H were displayed at 910 cm^{-1} and 829 cm^{-1}, respectively, demonstrating the formation of organic compounds such as phenols and alcohols during the pyrolysis of wheat straw (Li et al. 2020; Luo et al. 2019). The diffraction peak of FeS_2 appeared at 1132 cm^{-1} in S-nZVI/BC, indicating that the sulfidation was successful (Tang et al. 2021). The C-O (910 cm^{-1}) peak of BC was found to be weakened and the C-H peak was shifted from 829 to 814 cm^{-1} in the spectra of nZVI/BC and S-nZVI/BC, suggesting the binding of Fe^0 with

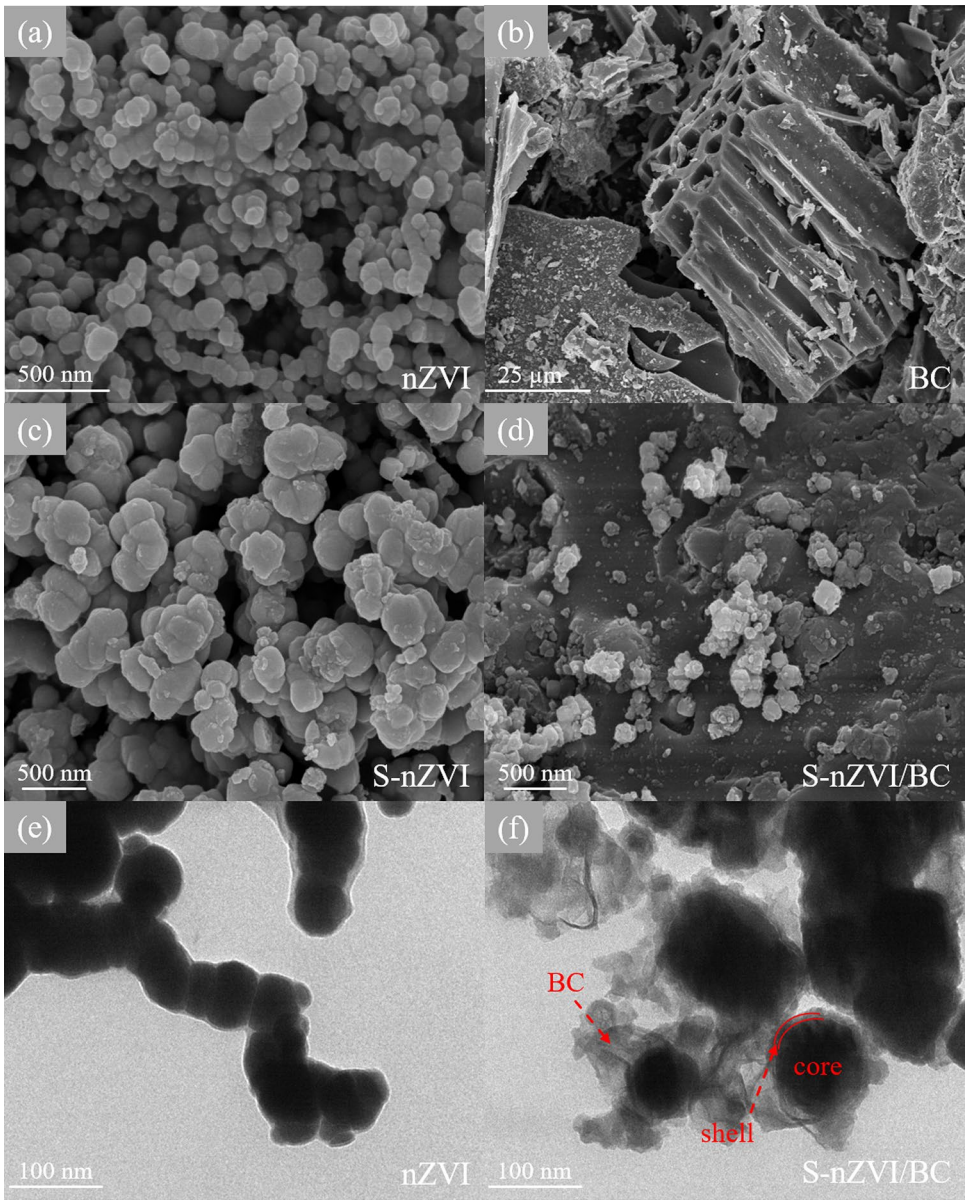

Fig. 2 SEM image of nZVI (**a**), BC (**b**), S-nZVI (**c**), S-nZVI/BC (**d**), and TEM image of nZVI (**e**), S-nZVI/BC (**f**)

some functional groups during the synthesis of composites (Luo et al. 2019). The FTIR analysis obtained coincides with the experimental data of SEM, TEM, and XPS. The above characterization results demonstrate the successful synthesis of S-nZVI/BC in this work.

According to the results of the elemental analysis (Table S2), S-nZVI and S-nZVI/BC materials had successfully been sulfidized as evidenced by the much higher S element content in comparison to nZVI, BC, and nZVI/BC. However, the S content of S-nZVI/BC decreased after BC supporting, but the C/H atomic ratio of nZVI/BC and S-nZVI/BC increased, demonstrating the efficacy of the supporting of nZVI and S-nZVI onto the BC surface. Moreover, to enhance understanding of nZVI, BC, nZVI/BC, S-nZVI, and S-nZVI/BC, their pH was measured before batch experiments (Table S3), with values of 8.60, 10.39, 8.91, 8.75, and 9.29, respectively.

3.2 Changes in the behavior of Cd

According to the BCR sequential extraction procedure, the stability of Cd speciation followed: residual > oxidizable > reducible > acid soluble (Rao et al. 2021). It was also observed that Cd speciation changed in soil during the treatment period, as shown in Fig. 4a. In the control group, the majority of the Cd speciation was acid soluble speciation which amounts to approximately 65.5%, while the percentage of reducible, oxidizable, and residual speciation were about 30.90%, 2.38%, and 1.22%, respectively. It indicates that Cd in the original soil has high mobility and

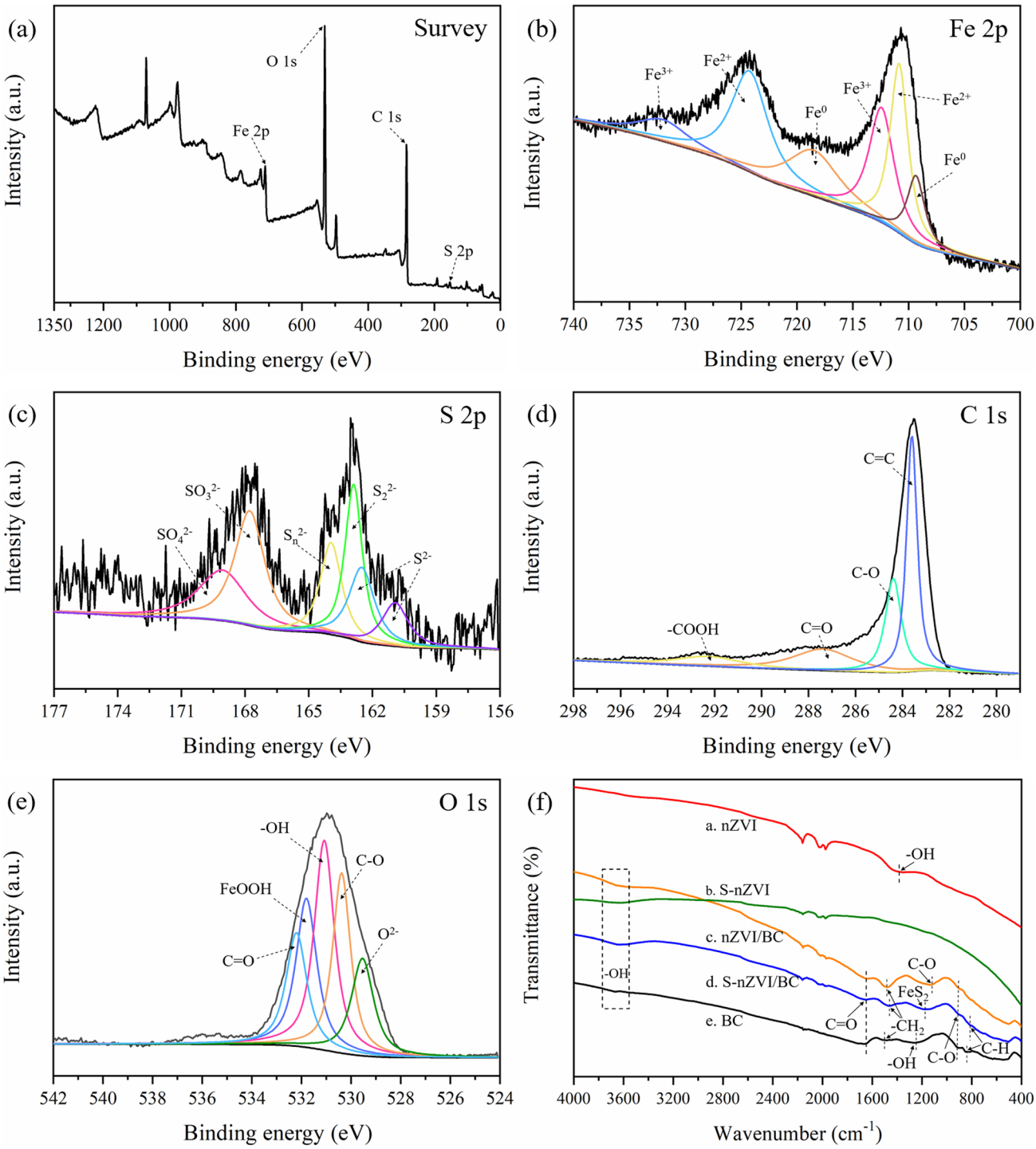

Fig. 3 XPS spectra of S-nZVI/BC: survey (**a**), Fe 2p (**b**), S 2p (**c**), C 1s (**d**), O1s (**e**), and FTIR spectra of S-nZVI/BC (**f**)

high environmental risk. The speciation distribution of Cd in each treatment group presented a similar change trend during the whole treatment period. From Fig. 4a, the oxidizable and residual speciation of Cd were time-dependent increased while the acid soluble speciation of Cd was time-dependent decreased, compared to the irregular change of Cd reducible speciation with time. As a result, the presence of nZVI, BC, nZVI/BC, S-nZVI, and S-nZVI/BC treatments significantly reduced by 19.77%, 15.92%, 26.95%, 25.52%, and 36.05% of the acid soluble of Cd after 49 days, respectively. On the contrary, the percentages of oxidizable speciation of Cd were elevated from 2.38% to 8.34%, 6.23%, 6.23%, 6.29%,

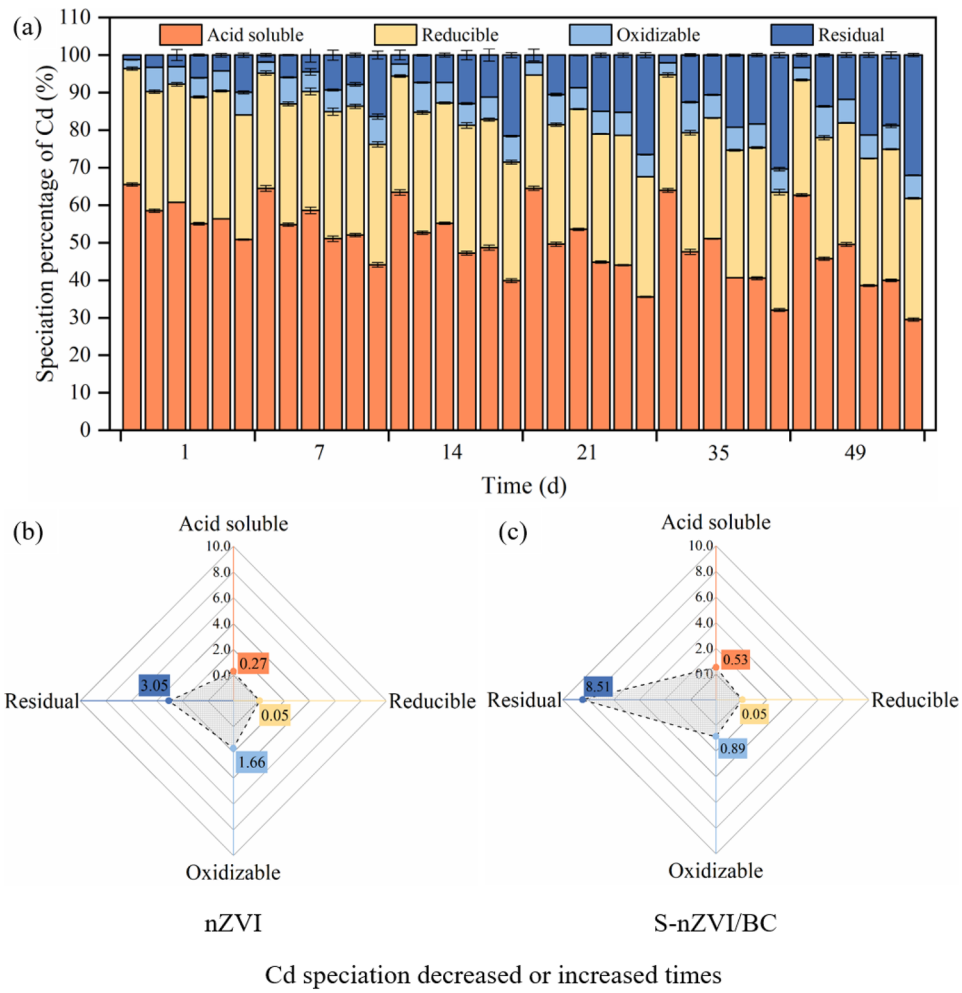

Fig. 4 **a** Change in the speciation of Cd during 49 days of treatment. (From left to right is control group, nZVI, BC, nZVI/BC, S-nZVI, S-nZVI/BC). The percentage of different speciation of Cd decreased or increased times with the treatment of nZVI (**b**) and S-nZVI/BC (**c**) at 49 days compared to control group. Error bars medicate standard deviation ($n = 3$)

and 6.16% and residual speciation increased from 1.22% to 13.68%, 11.84%, 21.32%, 18.83%, and 32.04% with the treatment of nZVI, BC, nZVI/BC, S-nZVI, and S-nZVI/BC, respectively. There was relatively less change in the percentages of reducible and oxidizable speciation compared to acid soluble and residual speciation, indicating that the acid soluble speciation was mainly transformed into the residual speciation after nanomaterials remediation. From Fig. 4b and c, the acid soluble speciation of Cd treated with nZVI and S-nZVI/BC was 0.27 and 0.53 times lower than the control group. The other Cd speciations (reducible, oxidizable, residual) also increased in the nZVI group compared to the control group by 0.05, 1.66, and 3.05 times (Fig. 4b), while the treatment of S-nZVI/BC was 0.05, 0.89, and 8.51 times (Fig. 4c), respectively. Thus, the addition of these nanomaterials effectively reduced mobility of Cd in soil, particularly when combined with S-nZVI/BC. At present, some amendments applications for the Cd remediation on soil contaminated were also reported by others, which was summarized in Table S4. For example, Yang et al. (2022) confirmed that compost palygorskite composite treatment increased the residual speciation of Cd by 7.74%. Song et al. (2022) investigated the soil Cd immobilization by biochar-supported nanoscale zero-valent iron (nZVI@BC) composite. Results indicated that the treatment of contaminated soil samples with nZVI@BC at a dosage of 3% (w/w) for 40 days increased Cd residual speciation by 9.26%. Ma et al. (2022b) demonstrated that the modified zeolite (MZEO) facilitated Cd immobilization in Baiyin soil, with a 15% increase in Cd residual specifications during 56 days of treatment. Compared to these amendments, S-nZVI/BC exhibited better Cd remediation effect, and its application could effectively reduce the mobility of Cd.

DTPA extraction was developed to predict heavy metal availability in soil. Figure 5a described the transformation of the DTPA-extractable Cd contents in the soil after treatment with different nanomaterials. The average amount of DTPA-extractable Cd in the control group essentially remained at 2.14 mg·kg^{-1} across the treatment process, with an initial content of DTPA-extractable Cd was 2.13 mg·kg^{-1} and a content of 2.16 mg·kg^{-1} after 49 days. Treatment groups had significantly lower levels of DTPA-extractable Cd than

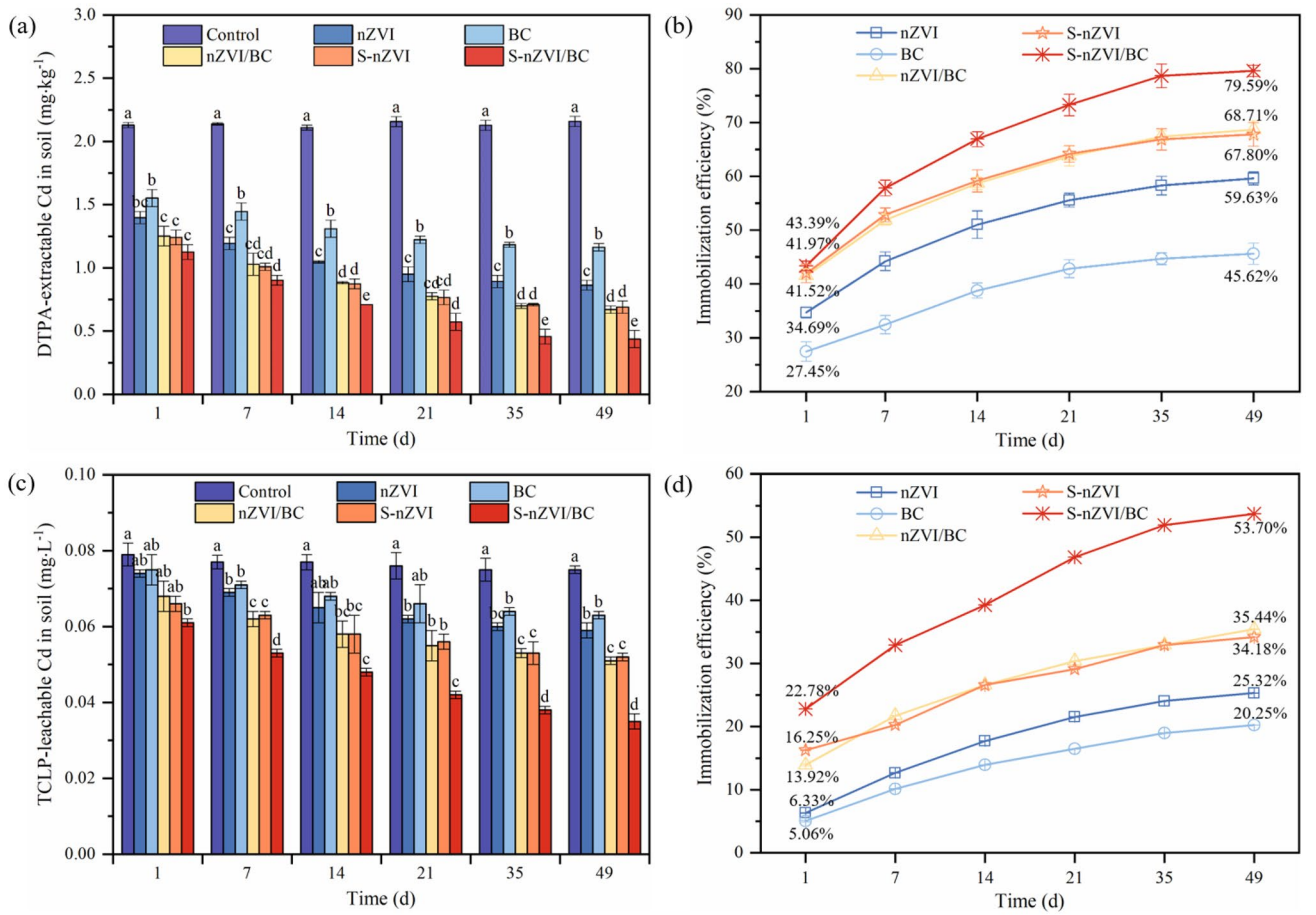

Fig. 5 Changes in content (**a**) and the immobilization efficiencies (**b**) of DTPA-extractable Cd, the concentration (**c**), and the immobilization efficiency (**d**) of TCLP-leachable Cd. Different lowercase letters represent significant differences within each treatment using one-way ANOVA ($p < 0.05$)

control groups ($P < 0.05$) and their levels decreased with each treatment day. From Fig. 5a, compared with control group, the DTPA-extractable Cd content were decreased by 1.28, 0.98, 1.47, 1.45, and 1.70 mg·kg^{-1} for nZVI, BC, nZVI/BC, S-nZVI, and S-nZVI/BC, respectively with the immobilization efficiencies of 45.62%, 59.63%, 67.80%, 68.71%, and 79.59% after 49 days of treatment, respectively (Fig. 5b). The result indicated that the addition of the nanomaterials diminished the content of DTPA-extractable Cd. Among them, S-nZVI/BC had the lowest DTPA-extractable Cd content and highest immobilization efficiencies, confirming that S-nZVI/BC displayed better immobilization potential to decrease the availability of Cd. Furthermore, the DTPA-extractable Cd content and percentages of acid soluble speciation exhibit basically the same trend of being lowered, going against the increasing tendency for the percentages of residual speciation. This situation concurred with the description of Fuentes et al. (2004), who reported that the acid soluble speciation obtained by BCR extraction was compared with the Cd content obtained by DTPA extraction, which could be pointed out that the change level of the metals was similar. Fan et al. (2020) also highlighted that the thiol-modified rice straw biochar increased Cd retention in soil complexing with mobilized Cd speciations, decreasing DTPA-extractable Cd levels. As a result, the lower amount of DTPA-extractable Cd showed that the activated Cd was transformed into a more stable species.

TCLP is usually employed to evaluate the performance of heavy metal leaching and migration in solid media. The variation of the TCLP-leachable Cd concentration and the immobilization efficiency in the soil treated with nanomaterials were exhibited in Fig. 5c and d. In the control group, it was found that the Cd concentration was slightly decreased, the initial TCLP-leachable Cd concentration was decreased from 0.079 to 0.075 mg·L^{-1} after 49 days of treatment. The concentration of TCLP-leachable Cd in soil was obviously lower after adding nanomaterials than the control group. From Fig. 5c, the concentration of TCLP-leachable Cd decreased to 0.059, 0.063, 0.051, 0.052, and 0.035 mg·L^{-1} for nZVI, BC, nZVI/BC, S-nZVI, and S-nZVI/BC, respectively, corresponding to 25.32%, 20.25%, 35.44%, 34.18%,

and 53.7% immobilization efficiencies ($P < 0.05$) (Fig. 5d), indicating that nZVI, BC, nZVI/BC, S-nZVI, and S-nZVI/BC may be able to reduce the biological toxicity of Cd in soil. S-nZVI/BC exhibited a superior immobilization capacity of TCLP-leachable Cd than nZVI, BC, nZVI/BC, and S-nZVI. The above analysis and discussions suggested that nanomaterials could contribute to effectively decreasing TCLP-extractable Cd concentration, reducing the dissolution of Cd in soils, and thereby reducing the environmental risk.

This study also synthesized four micromaterials, i.e., micro zero-valent iron (mZVI), BC supported mZVI (mZVI/BC), sulfurized mZVI (S-mZVI), and BC supported S-mZVI (S-mZVI/BC), for the immobilization of Cd in paddy soil. The characterization results of the micromaterials and the immobilization effect on Cd were shown in Figs. S1 and S2, respectively. Results indicated that micromaterials could reduce the content of DTPA-extractable Cd and the leaching toxicity of Cd, but were not as effective as nanomaterials.

3.3 Changes of pH, Eh, and OM in paddy soil

It is widely accepted that soil pH has a significant effect on the mobility of heavy metals (Xu et al. 2021). Usually, lower pH decreases the Cd adsorption on soil colloids by reducing the negative charge carried by soil colloids, which enhances the mobility of Cd (Liu et al. 2022). Hence, Fig. 6a represented the change in soil pH during the course of the 49 days treatment. The pH of the control group remained unchanged basically in the treatment process, which was approximately 7.57 ± 0.03. Compared to control group, the application of nZVI, BC, nZVI/BC, S-nZVI, and S-nZVI/BC considerably higher soil pH on the first day, corresponding to increase from 7.57 to 8.50, 7.82, 8.10, 8.52, and 8.36, respectively ($P < 0.05$). The alkaline characteristics of BC and the production of OH^- by the oxidation process of Fe^0 were the main increased causes of pH (Gong et al. 2021). In addition, it was observed that the change of pH in other treatment groups during 49 days was irregular. It has been reported that OH^- could combine with dissolved metal ions to release H^+, reducing the soil pH (Li et al. 2019). Moreover, the pH decreases in nZVI and modified nZVI treatment groups may be attributed to the hydrolysis of dissolved iron ions (Li et al. 2019). Specifically, Cd and HS^- formed CdS also released H^+ in the S-nZVI and S-nZVI/BC treatment groups (Liang et al. 2022). However, compared to the blank group, the pH of the treated group was higher during the whole treatment process. After 49 days, the pH values of nZVI, BC, nZVI/BC, S-nZVI, and S-nZVI/BC treatment groups were 8.35, 8.25, 8.28, 8.46, and 8.26, and increased by 0.76, 0.66, 0.69, 0.87, and 0.67 units compared with control group, respectively. The pH of each treatment group was still high than 8 after 49 days of treatment. It has been revealed that the formation of Cd hydroxyl substances occurred at $pH \geq 8$ (Xue et al. 2018). On the other hand, the negative charge of the nanomaterials increased at high pH, enhancing the electrostatic affinity to positively charged metal ions and strengthening the adsorption and complexation, which facilitated the immobilization of Cd (Yang et al. 2021c).

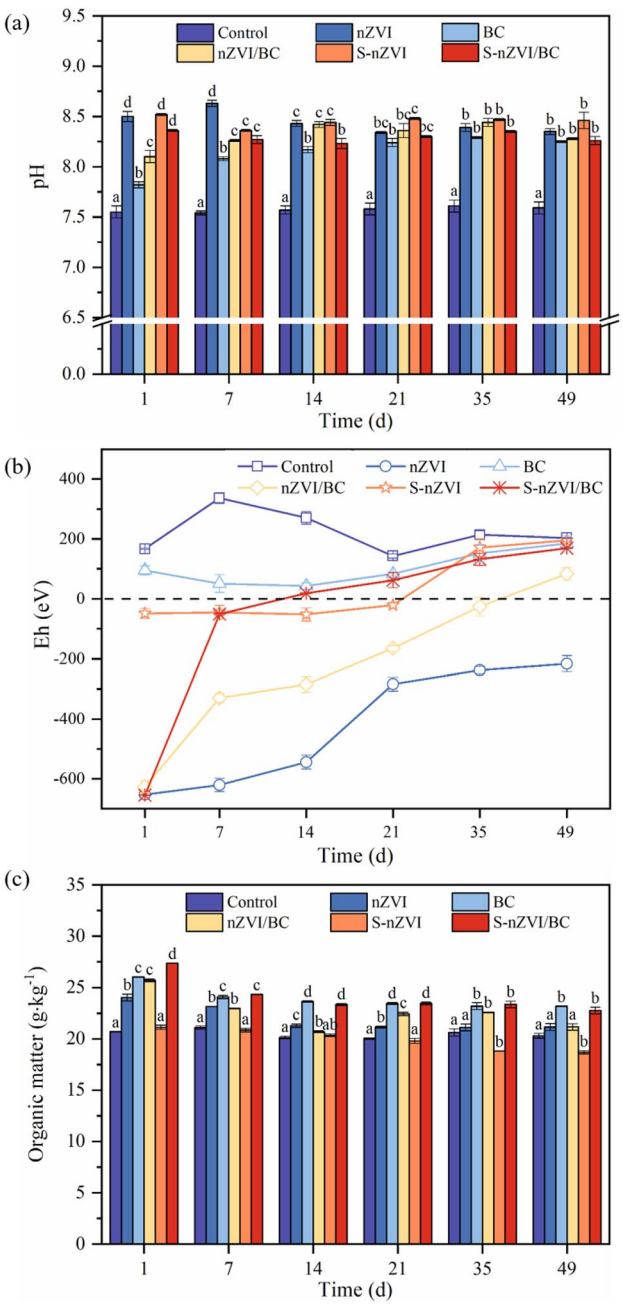

Fig. 6 Changes of pH (**a**), Eh (**b**), and OM (**c**) during 49 days of treatment in amendment soil. Different lowercase letters represent significant differences within each treatment using one-way ANOVA ($p < 0.05$)

Changes of soil Eh will lead to changes in soil redox conditions, which will further influence the transformation of heavy metals (Yao et al. 2022). It was observed from

Fig. 6b that the Eh of the control group increased firstly and then decreased during the treatment period. The Eh value increased by only 36 mV after 49 days of treatment compared to the Eh value on the first days. The reason for this phenomenon might be that, when soil samples were submerged at the early stage, there were microorganisms that could serve as a medium for oxygen transfer from the water, thereby contributing to the maintenance of soil oxidation state. However, with the intensification of aerobic microbial activity in the soil, oxygen is progressively depleted, causing a corresponding decrease in Eh values (He et al. 2022). After adding nZVI, BC, nZVI/BC, S-nZVI, and S-nZVI/BC to the contaminated soil samples, the Eh values of the nZVI, nZVI/BC, and S-nZVI/BC treatment groups were in a strong reducing state on the first days, at − 652, − 626, and − 654 mV, respectively. Then, they gradually increased over time, and the values were − 216, 83, and 169 mV after 49 days, respectively. The Eh values of the BC and S-nZVI treatment groups gradually decreased in the early stage but began to rise after 14 days. The changes of Eh were not only related to the effects of microbial transport and oxygen consumption mentioned earlier but also speculated to be related to the release and hydrolysis of Fe^{2+} (Crane and Sapsford 2018). When the soil was in a reducing state, it became easy for Cd to combine with sulfides to form insoluble CdS, and the adsorption/co-precipitation effect of Fe–Mn (oxyhydro) oxides on Cd was enhanced, ultimately reducing its mobility. Furthermore, secondary Fe minerals formed by the anaerobic oxidation of Fe(II) could effectively adsorb free Cd (Wang et al. 2019). Over time, Fe^{2+} was oxidized to form Fe^{3+}, and the Eh of each treatment group increased (Shen et al. 2020). With the increase of Eh value, sulfide-bound Cd may be released, and the released Cd^{2+} can then be further stabilized by the nanomaterial (Chen et al. 2020). The soil gradually transitioned to an oxidized state, but the Eh values of each treatment group were lower than those of the control group throughout the treatment period.

As shown in Fig. 6b, the OM content of the control group was lower than that of each treatment group during the first day. As already mentioned, BC was prepared by high-temperature pyrolysis of wheat straw in this experiment. It not only contained a high carbon content but also exhibited strong adsorption potential for organic molecules, increasing the content of soil OM (Fan et al. 2020; Zhang et al. 2022a). For nZVI, it released iron ions which may be combined with water-soluble substances in the solid phase to enhance the soil OM content (Hui et al. 2021). Furthermore, the sulfidation reduced the release of Fe^{2+} in S-nZVI and most of the Fe^{2+} ions were entrapped in the outer layer of the particles (Cheng et al. 2019), so the OM content of S-nZVI treatment group only increased by 0.23 $mg \cdot kg^{-1}$ compared with the control group. After that, the OM content in each treatment group showed a downward trend and become stable. The OM content was 21.15, 23.80, 21.16, 18.76, and 22.76 $mg \cdot kg^{-1}$, respectively, for nZVI, BC, nZVI/BC, S-nZVI, and S-nZVI/BC, which were higher than control group (20.30 $mg \cdot kg^{-1}$) except for S-nZVI. This might be attributed to the increased OM content promoting microbial activities in soil (Wang et al. 2021b). Moreover, the changes in Cd speciations indicated that the nanomaterials could gradually facilitate the transfer of mobility speciation to stable speciations and decrease Cd toxicity (Kong and Lu 2022), altering soil microbial community structures and functions, promoting the activity of some microorganisms that decompose OM, thus reducing the content of OM (Xu et al. 2021).

To further explore the relationship between soil properties and heavy metal mobility, Pearson correlation analysis among the Cd speciation, the content of extracted Cd, and pH, Eh, and OM were shown in Table 1. The pH showed significant negative correlation with the Cd acid soluble speciation and the DTPA-extractable Cd, while a significant positive correlation with the Cd oxidation speciation, with correlation coefficients of − 0.823 ($P < 0.05$), − 0.930 ($P < 0.01$), and 0.836 ($P < 0.05$), suggesting that the increase of pH could decrease the mobility of Cd, and then reduced the environmental risk of Cd. There was a negative correlation between the Eh and the Cd oxidation speciation, with a correlation coefficient of − 0.919 ($P < 0.01$). The soil Eh value of each treatment group was lower than that of the control group during the 49 days of treatment, corresponding to the increase of the Cd oxidation speciation in the previous BCR sequential extraction, which proved that the decrease of Eh value could promote the Cd mobility to stable state. OM could directly adsorb and complex with Cd, or indirectly affect the immobilization of Cd by promoting the dissolution of iron oxides and co-precipitating/complexation with iron oxides to produce organic matter-iron oxide complexes (Bao et al. 2022). However, no significant relationships were observed between soil OM and Cd in each speciation, or even the extracted Cd concentrations, which indicated that

Table 1 Pearson correlation analysis among the Cd speciation, the content of extracted Cd, and soil pH, Eh and OM

	Acid soluble	Reducible	Oxidizable	Residual	DTPA	TCLP
pH	− 0.823*	0.712	0.836*	0.690	− 0.930**	− 0.706
Eh	0.441	− 0.392	− 0.919**	− 0.284	0.621	0.363
OM	− 0.257	− 0.383	0.111	0.340	− 0.229	− 0.312

*Correlation is significant at the 0.05 level; **Correlation is significant at the 0.01 level

variation in soil OM had limited effect on Cd transformation with nanomaterial treatment. DTPA-extractable Cd had a considerably negative correlation with pH ($P < 0.01$). These indicated that an increase in pH facilitated the transition of Cd to the residual speciation, which reduced the toxicity and availability of Cd. In short, soil pH was the major factor of Cd mobility in soil.

3.4 Characterization of nanomaterials after remediation

Investigations into the magnetically separated particles isolated from the treated paddy soil after the reaction were studied to further explore the possible stabilization mechanism of Cd by S-nZVI/BC in soil. Those investigations included SEM, FTIR, and X-ray diffraction (XRD). Figure 7 presented the SEM images and corresponding energy dispersive spectrometry (EDS) mapping of S-nZVI/BC particles separated after reacting with Cd for 49 days. Compared with the original S-nZVI/BC (Fig. 2d), the S-nZVI/BC surface became rougher after the reaction, most of the particles were mainly comprised flaky and a litter rough spherical structure (Fig. 7a). The EDS mapping of C, O, S, Fe, and Cd was displayed in Fig. 7b–f. The distribution of Cd was clearly matched with Fe, O, and S, which illustrated that Fe, O, and S were the key elements for Cd adsorption. Furthermore, the EDS analysis revealed that the particles were mainly composed of C (12.36%), O (55.28%), S (0.08%), Fe (23.29%), and Cd (8.99%) (Fig. 7g), indicating that Cd was successfully enriched by S-nZVI/BC. Thus, it was conjectured that the soluble Cd was immobilized in the paddy soil by reacting with FeS_x on the S-nZVI/BC surface to form CdS with low solubility, and/or the formation of complexes with iron oxide/hydroxide (Liang et al. 2021a).

S-nZVI/BC before and after the reaction was further analyzed using FTIR spectroscopy to reveal the changes in functional groups (Fig. 8a). All the bands were shown at 3700–3400 cm^{-1} as the result of O–H stretching vibration (Tang et al. 2021), the O–H peak after the remediation of Cd was sharper at 3632 cm^{-1} and a new O–H peak appeared at 3440 cm^{-1} (Dong et al. 2017; Tang et al. 2021), probably due to the oxidation and hydrolysis of Fe^0 to produce more iron hydroxide (e.g., FeOOH) (Hui et al. 2022), as well as the combination of Cd^{2+} with hydroxyl groups to form various hydroxyl compounds (e.g., $Cd(OH)_2$) (Liang et al. 2022). The C = O vibration peak of the functional group from 1667 to 1652 cm^{-1}, presumably resulting in the changes caused by the complexation of Cd with functional groups in BC structures during soil remediation. The Cd–O vibration peak was located at 1440 cm^{-1}, confirming the stabilization of Cd^{2+} on S-nZVI/BC by adsorption and/or complexation (He et al. 2022). Additionally, the characteristic peak at 1039 cm^{-1} was observed after remediation, probably corresponding to the stretching vibration of hydrated ferric sulfate, indicating the possible existence of sulfate ions in the S-nZVI/BC (Hui et al. 2022). Moreover, the Fe–O vibration peaks were observed after remediation at 698, 534, and 470 cm^{-1}, inferring that more iron oxides were formed due to the oxidation of Fe^0 (Gu et al. 2021; Liang et al. 2021a).

The XRD patterns were conducted to determine the changes in chemical transformation of S-nZVI/BC before and after remediation of Cd-contaminated paddy soil.

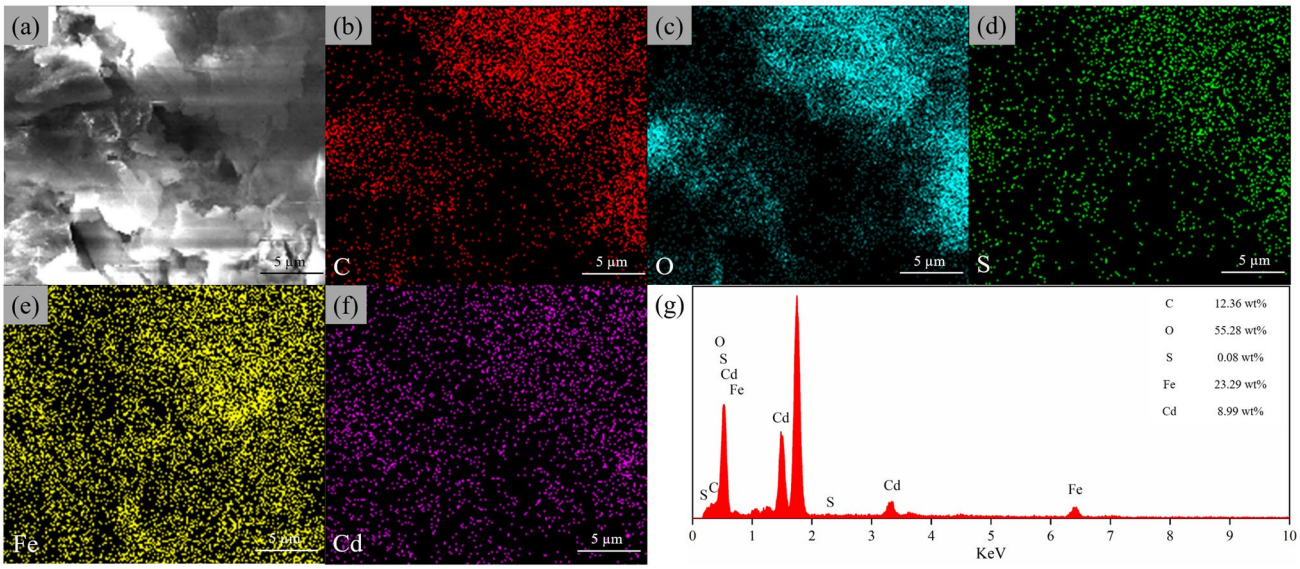

Fig. 7 The SEM images (**a**) of S-nZVI/BC after reaction with Cd, and the corresponding mapping of C (**b**), O (**c**), S (**d**), Fe (**e**), Cd (**f**), and EDS (**g**)

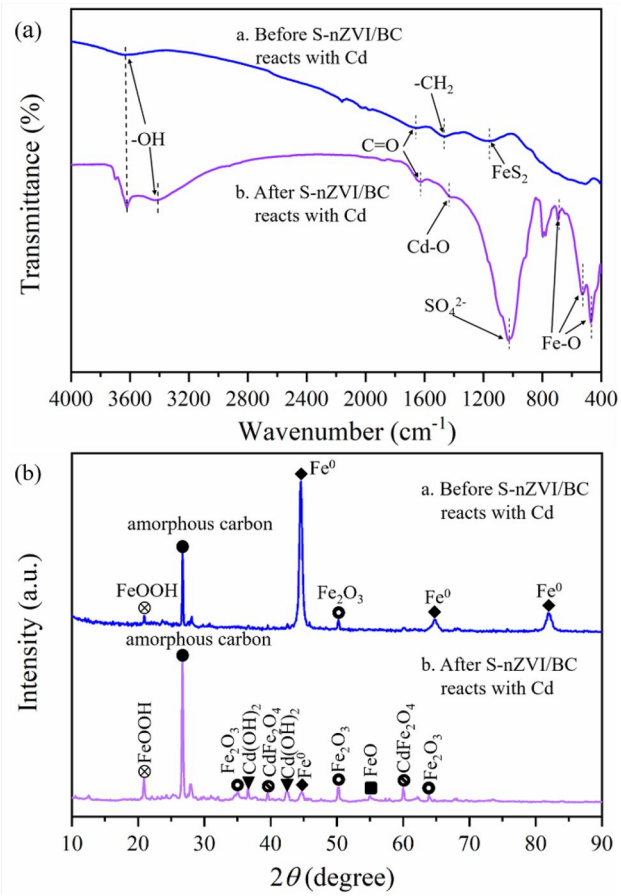

Fig. 8 FTIR spectra (**a**) and XRD (**b**) of S-nZVI/BC before and after reaction with Cd

According to Fig. 8b, the XRD analysis of S-nZVI/BC before remediation showed an apparent characteristic peak of Fe^0 ($2\theta = 44.9°$, 65.0°, 82.1°) (Gao et al. 2022a; Yang et al. 2021b), and iron oxide/hydroxide peaks at $2\theta = 21.1°$ (FeOOH) and $2\theta = 50.3°$ (Fe_2O_3) (Liang et al. 2022; Yang et al. 2021b). It was inevitable that part of Fe^0 in the nanomaterials was oxidized. The amorphous carbon of BC was observed at $2\theta = 26.7°$, which indicated that BC successfully supports S-nZVI (Hamid et al. 2022). The peaks associated with sulfur-containing compounds (e.g., FeS or FeS_2) were not observed, probably due to their low crystallinity (Gao et al. 2020). Compared with the pristine S-nZVI/BC, the XRD patterns of S-nZVI/BC after treatment observed the intensity of the special peak at $2\theta = 44.9°$ for Fe^0 was weakened and $2\theta = 65.0°$, 82.1° of Fe^0 almost disappeared. In contrast, the distinct peaks located at $2\theta = 21.1°$ for FeOOH, and $2\theta = 50.3°$ for Fe_2O_3 were enhanced, while some diffraction peaks at $2\theta = 54.8°$ for FeO and $2\theta = 63.9°$ for Fe_2O_3 were discovered (He et al. 2022). These iron oxide/hydroxide are beneficial to provide more reaction sites for immobilizing free Cd in soil via adsorption, complexation, and other mechanisms (Dong et al. 2017). Moreover, some novel characteristic peaks of $Cd(OH)_2$ ($2\theta = 36.7°$, 42.6°) and $CdFe_2O_4$ ($2\theta = 39.2°$, 60.0°) were found, which confirmed precipitation and complexation were detected for Cd stabilization (Ainiwaer et al. 2022; He et al. 2022; Yang et al. 2021b).

3.5 Immobilization mechanism

Based on the characterization of the separated S-nZVI/BC after remediation, it was determined that the remediation mechanism of Cd included adsorption, complexation, and precipitation processes (Fig. 9). Firstly, alkaline biochar had more negative charges on its surface, which increased the electrostatic interaction between the nanomaterials and Cd (Liang et al. 2022). The abundant functional groups on the S-nZVI/BC influenced Cd adsorption through promote the formation of Cd compounds (Eqs. (2–3)) (Liang et al. 2022). Secondly, Fe^0 in S-nZVI/BC was easily converted into various iron oxide/hydroxide in soil under suitable soil conditions. According to the XRD results, the oxidation product types of Fe were mainly FeOOH and Fe_2O_3, which possessed high adsorption capacity (Eqs. (4–6)) (Hui et al. 2022). It

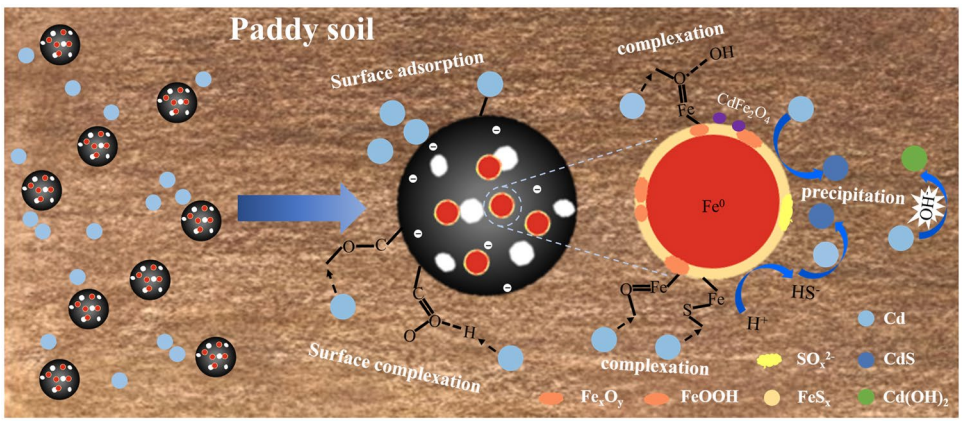

Fig. 9 A schematic of the possible reaction mechanism of Cd by S-nZVI/BC

provided the adsorption sites for the surface complexation of iron oxide/hydroxide with Cd ($FeOCd^+$, FeOCdOH) (Eqs. (7–8)), which was confirmed by some researchers (Liang et al. 2022). Then, Cd could replace Fe^{2+} from FeS to form CdS precipitation with lower solubility (Eq. (9)) (Liang et al. 2020). Also, Cd could react with the dissolved S ions to form CdS (Eqs. (10–11)) (Gao et al. 2022b). Furthermore, it was also possible that the surface complexation of FeS_x layer reaction with Cd ($FeS\text{-}Cd^{2+}$) (Eq. (12)) (Liang et al. 2022). In addition, the incorporation of nanomaterials raises soil pH and promotes the formation of insoluble $Cd(OH)_2$ from Cd^{2+} and OH^- (Yang et al. 2021b). Furthermore, the generation secondary iron mineral ($CdFe_2O_4$) had strong complexing ability to Cd (He et al. 2022).

$$C - OH + Cd^2 \rightarrow C - OCd^+ + H^+ \quad (2)$$

$$2C - COOH + Cd^{2+} \rightarrow (C - COO)_2Cd + 2H^+ \quad (3)$$

$$Fe^0 + 2H_2O \rightarrow Fe^{2+} + H_2 + 2OH^- \quad (4)$$

$$4Fe^{2+} + O_2 + 2H_2O \rightarrow 4Fe^{3+} + 4OH^- \quad (5)$$

$$4Fe^0 + O_2 + 2H_2O \rightarrow 4FeOOH \quad (6)$$

$$FeO^- + Cd^{2+} \rightarrow FeOCd^+ \quad (7)$$

$$FeOH + Cd^2 + H_2O \rightarrow FeOCdOH + 2H^+ \quad (8)$$

$$FeS + Cd^{2+} \rightarrow Fe^{2+} + CdS \quad (9)$$

$$FeS + H^+ \rightarrow Fe^{2+} + HS^- \quad (10)$$

$$HS^- + Cd^{2+} \rightarrow H^+CdS \quad (11)$$

$$FeSH^- + Cd^{2+} \rightarrow FeS - Cd^+ + H^+ \quad (12)$$

4 Conclusion

S-nZVI/BC composites were synthesized and employed in this investigation for Cd immobilization in contaminated paddy soil. The synthesized products were characterized by SEM, TEM, XPS, and FTIR. These results confirmed that S-nZVI/BC had excellent dispersity, and the S-nZVI particles showed an obvious shell-core structure with Fe^0 as the core and FeS_x, sulfur oxides, and a small amount of iron oxide/hydroxide in the shell. Remediation tests in the paddy soil determined that S-nZVI/BC could effectively convert the acid soluble speciation of Cd to residual speciation. At the same time, DTPA-extractable Cd availability and TCLP-leachable Cd leachability were significantly decreased. Moreover, it was verified that the increase in soil pH caused by the addition of S-nZVI/BC could decrease the mobility of Cd. The immobilization mechanism of Cd clarified that surface adsorption or complexation on the formed iron oxide/hydroxide or FeS_x layer and secondary iron mineral, precipitation to form CdS and $Cd(OH)_2$. Furthermore, this study estimated the material cost of adding 3% S-nZVI/BC to 1 g of soil to be 0.207 RMB. Therefore, using S-nZVI/BC to remediate actual Cd-contaminated soil has economic feasibility. These findings provide evidence on behalf of the employment of nanoscale zero-valent iron nanocomposites for heavy metal remediation in contaminated soils.

Supplementary Information The online version contains supplementary material available at https://doi.org/10.1007/s11368-023-03618-4.

Funding This work was financially supported by the Program for the National Natural Science Foundation of China (42107415) and Natural Science Foundation of Jiangsu Province (BK20210830).

Data availability Data is available upon request.

Declarations

Competing interests The authors declare no competing interests.

References

Ainiwaer M, Zhang T, Zhang N, Yin X, Su S, Wang Y, Zhang Y, Zeng X et al (2022) Synergistic removal of As(III) and Cd(II) by sepiolite-modified nanoscale zero-valent iron and a related mechanistic study. J Environ Manage 319:115658. https://doi.org/10.1016/j.jenvman.2022.115658

Bao Y, Bolan NS, Lai J, Wang Y, Jin X, Kirkham M, Wu X, Fang Z, Zhang Y, Wang HL et al (2022) Interactions between organic matter and Fe (hydr)oxides and their influences on immobilization and remobilization of metal(loid)s: a review. Crit Rev Environ Sci Technol 52:4016–4037. https://doi.org/10.1080/10643389.2021.1974766

Bhattacharjee S, Ghoshal S (2018) Optimal design of sulfidated nanoscale zerovalent iron for enhanced trichloroethene degradation. Environ Sci Technol 52:11078–11086. https://doi.org/10.1021/acs.est.8b02399

Chen H, Wang P, Gu Y, Kretzschmar R, Kopittke P, Zhao F et al (2020) The within-field spatial variation in rice grain Cd concentration is determined by soil redox status and pH during grain filling. Environ Poll 261:114151. https://doi.org/10.1016/j.envpol.2020.114151

Cheng Y, Dong H, Lu Y, Hou K, Wang Y, Ning Q, Li L, Wang B, Zhang L, Zeng G et al (2019) Toxicity of sulfide-modified nanoscale zero-valent iron to *Escherichia coli* in aqueous solutions. Chemosphere 220:523–530. https://doi.org/10.1016/j.chemosphere.2018.12.159

Crane R, Sapsford D (2018) Towards "Precision Mining" of wastewater: selective recovery of Cu from acid mine drainage onto diatomite supported nanoscale zerovalent iron particles. Chemosphere 202:339–348. https://doi.org/10.1016/j.chemosphere.2018.03.042

Dong H, Deng J, Xie Y, Zhang C, Jiang Z, Cheng Y, Hou K, Zeng G et al (2017) Stabilization of nanoscale zero-valent iron (nZVI) with modified biochar for Cr(VI) removal from aqueous solution. J Hazard Mater 332:79–86. https://doi.org/10.1016/j.jhazmat.2017.03.002

Dong Q, Dong H, Li Y, Xiao J, Xiang S, Hou X, Chu D et al (2022) Degradation of sulfamethazine in water by sulfite activated with zero-valent Fe-Cu bimetallic nanoparticles. J Hazard Mater 431:128601. https://doi.org/10.1016/j.jhazmat.2022

Fan J, Cai C, Chi H, Reid BJ, Coulon F, Zhang Y, Hou Y et al (2020) Remediation of cadmium and lead polluted soil using thiol-modified biochar. J Hazard Mater 388:122037. https://doi.org/10.1016/j.jhazmat.2020.122037

Fan Y, Huang L, Wu L, Zhang C, Zhu S, Xiao X, Li M, Zou X et al (2021) Adsorption of sulfonamides on biochars derived from waste residues and its mechanism. J Hazard Mater 406:124291. https://doi.org/10.1016/j.jhazmat.2020.124291

Fan T, Yao X, Sun Z, Sang D, Liu L, Deng H, Zhang Y et al (2023) Properties and metal binding behaviors of sediment dissolved organic matter (SDOM) in lakes with different trophic states along the Yangtze River Basin: a comparison and summary. Water Res 231:119605. https://doi.org/10.1016/j.watres.2023.119605

Fuentes A, Llorens M, Saez J, Soler A, Aguilar MI, Ortuno JF, Meseguer VF et al (2004) Simple and sequential extractions of heavy metals from different sewage sludges. Chemosphere 54:1039–1047. https://doi.org/10.1016/j.chemosphere.2003.10.029

Gao F, Ahmad S, Tang J, Zhang C, Li S, Yu C, Liu Q, Sun H et al (2022a) Enhanced nitrobenzene removal in soil by biochar supported sulfidated nano zerovalent iron: solubilization effect and mechanism. Sci Total Environ 826:153960. https://doi.org/10.1016/j.scitotenv.2022.153960

Gao J, Han D, Xu Y, Liu Y, Shang J et al (2020) Persulfate activation by sulfide-modified nanoscale iron supported by biochar (S-nZVI/BC) for degradation of ciprofloxacin. Sep Purif Technol 235:116202. https://doi.org/10.1016/j.seppur.2019.116202

Gao R, Hu P, Dai Y, Zhang Y, Liu L, Yang W et al (2022b) Removal of cadmium(II) from aqueous solutions by a novel sulfide-modified nanoscale zero-valent iron supported on kaolinite: treatment efficiency, kinetics and mechanisms. Appl Surf Sci 602:154353. https://doi.org/10.1016/j.apsusc.2022.154353

Gong X, Huang D, Liu Y, Zou D, Hu X, Zhou L, Wu Z, Yang Y, Xiao Z et al (2021) Nanoscale zerovalent iron, carbon nanotubes and biochar facilitated the phytoremediation of cadmium contaminated sediments by changing cadmium fractions, sediments properties and bacterial community structure. Ecotox Environ Saf 208:111510. https://doi.org/10.1016/j.ecoenv.2020.111510

Gu H, Gao Y, Xiong M, Zhang D, Chen W, Xu Z et al (2021) Removal of nitrobenzene from aqueous solution by graphene/biochar supported nanoscale zero-valent-iron: reduction enhancement behavior and mechanism. Sep Purif Technol 275:119146. https://doi.org/10.1016/j.seppur.2021.119146

Hamid Y, Liu L, Usman M, Naidu R, Haris M, Lin Q, Ulhassan Z, Hussain MI, Yang X et al (2022) Functionalized biochars: synthesis, characterization, and applications for removing trace elements from water. J Hazard Mater 437:129337. https://doi.org/10.1016/j.jhazmat.2022.129337

Han Y, Ghoshal S, Lowry GV, Chen J et al (2019) A comparison of the effects of natural organic matter on sulfidated and nonsulfidated nanoscale zerovalent iron colloidal stability, toxicity, and reactivity to trichloroethylene. Sci Total Environ 671:254–261. https://doi.org/10.1016/j.scitotenv.2019.03.343

He Y, Fang T, Wang J, Liu X, Yan Z, Lin H, Li F, Guo G et al (2022) Insight into the stabilization mechanism and long-term effect on As, Cd, and Pb in soil using zeolite-supported nanoscale zero-valent iron. J Clean Prod 355:131634. https://doi.org/10.1016/j.jclepro.2022.131634

Hu YB, Ma L, Yuan B, Li XY et al (2021) Confining polyacrylic acid on the surface of nanoscale zero-valent iron by aluminum hydroxide for in-situ anti-passivation. J Hazard Mater 420:126649. https://doi.org/10.1016/j.jhazmat.2021.126649

Huang H, Zhao D, Wang P et al (2021) Biogeochemical control on the mobilization of Cd in soil. Curr Pollution Rep 7:194–200. https://doi.org/10.1007/s40726-021-00180-w

Huang J, Li Z, Zhang J, Zhang Y, Ge Y, Cui X et al (2020) In-situ synchronous carbonation and self-activation of biochar/geopolymer composite membrane: enhanced catalyst for oxidative degradation of tetracycline in water. Chem Eng J 397:125528. https://doi.org/10.1016/j.cej.2020.125528

Hui C, Liu B, Du L, Xu L, Zhao Y, Shen D, Long Y et al (2022) Transformation of sulfidized nanoscale zero-valent iron particles and its effects on microbial communities in soil ecosystems. Environ Pollut 306:119363. https://doi.org/10.1016/j.envpol.2022.119363

Hui C, Zhang Y, Ni X, Cheng Q, Zhao Y, Zhao Y, Du L, Jiang H et al (2021) Interactions of iron-based nanoparticles with soil dissolved organic matter: adsorption aging, and effects on hexavalent chromium removal. J Hazard Mater 406:124650. https://doi.org/10.1016/j.jhazmat.2020.124650

Jiang M, Wang K, Li G, Zhao Q, Wang W, Jiang J, Wang Y, Yuan L et al (2022a) Stabilization of arsenic, antimony, and lead in contaminated soil with montmorillonite modified by ferrihydrite: efficiency and mechanism. Chem Eng J 457:141182. https://doi.org/10.1016/j.cej.2022.141182

Jiang Q, Jiang S, Li H, Zhang R, Jiang Z, Zhang Y et al (2022b) A stable biochar supported S-nZVI to activate persulfate for effective dichlorination of atrazine. Chem Eng J 431:133937. https://doi.org/10.1016/j.cej.2021.133937

Jin Y, Wang Y, Li X, Luo T, Ma Y, Wang B, Liang H et al (2023) Remediation and its biological responses to Cd(II)-Cr(VI)-Pb(II) multi-contaminated soil by supported nano zero-valent iron composites. Sci Total Environ 867:161344. https://doi.org/10.1016/j.scitotenv.2022.161344

Khan ZH, Gao M, Wu J, Bi R, Mehmood CT, Song Z et al (2021) Mechanism of As(III) removal properties of biochar-supported molybdenum-disulfide/iron-oxide system. Environ Pollut 287:117600. https://doi.org/10.1016/j.envpol.2021.117600

Kong F, Lu S (2022) Effects of microbial organic fertilizer (MOF) application on cadmium uptake of rice in acidic paddy soil: regulation of the iron oxides driven by the soil microorganisms. Environ Pollut 307:119447. https://doi.org/10.1016/j.envpol.2022.119447

Li X, Yang Z, Zhang C, Wei J, Zhang H, Li Z, Ma C, Wang M, Chen J, Hu J et al (2019) Effects of different crystalline iron oxides on immobilization and bioavailability of Cd in contaminated sediment. Chem Eng J 373:307–317. https://doi.org/10.1016/j.cej.2019.05.015

Li Y, Zhang X, Zhang P, Liu X, Han L et al (2020) Facile fabrication of magnetic bio-derived chars by co-mixing with Fe_3O_4 nanoparticles for effective Pb^{2+} adsorption: properties and mechanism. J Clean Prod 262:121350. https://doi.org/10.1016/j.jclepro.2020.121350

Liang L, Li X, Lin Z, Tian C, Guo Y et al (2020) The removal of Cd by sulfidated nanoscale zero-valent iron: the structural, chemical bonding evolution and the reaction kinetics. Chem Eng J 382:122933. https://doi.org/10.1016/j.cej.2019.122933

Liang L, Li W, Li Y, Zhou W, Chen J et al (2021a) Removal of EDTA-chelated Cd(II) by sulfidated nanoscale zero-valent iron: removal mechanisms and influencing factors. Sep Purif Technol 276:119332. https://doi.org/10.1016/j.seppur.2021.119332

Liang L, Li X, Guo Y, Lin Z, Su X, Liu B et al (2021b) The removal of heavy metal cations by sulfidated nanoscale zero-valent iron (S-nZVI): the reaction mechanisms and the role of sulfur. J Hazard Mater 404:124057. https://doi.org/10.1016/j.jhazmat.2020.124057

Liang W, Shen Y, Xu C, Cai D, Wang D, Luo K, Shao X, Qiao Z, Zhang W, Peng C et al (2022) Enhanced simultaneous removal of Cr(VI) and Cd(II) from aqueous solution and soil: a novel carbon microsphere–calcium alginate supported sulfide-modified nZVI composite. Environ Sci: Nano 9:2051–8153. https://doi.org/10.1039/d2en00483f

Liu M, Wang J, Xu M, Tang S, Zhou J, Pan W, Ma Q, Wu L et al (2022) Nano zero-valent iron-induced changes in soil iron species and soil bacterial communities contribute to the fate of Cd. J Hazard Mater 424:127343. https://doi.org/10.1016/j.jhazmat.2021.127343

Liu M, Xu M, Zhang X, Zhou J, Ma Q, Wu L et al (2021) Poorly crystalline Fe(II) mineral phases induced by nano zero-valent iron are responsible for Cd stabilization with different soil moisture conditions and soil types. Ecotox Environ Saf 223:112616. https://doi.org/10.1016/j.ecoenv.2021.112616

Liu SJ, Liu YG, Tan XF, Zeng GM, Zhou YH, Liu SB, Yin ZH, Jiang LH, Li MF, Wen J et al (2018) The effect of several activated biochars on Cd immobilization and microbial community composition during in-situ remediation of heavy metal contaminated sediment. Chemosphere 208:655–664. https://doi.org/10.1016/j.chemosphere.2018.06.023

Luo H, Lin Q, Zhang X, Huang Z, Liu S, Jiang J, Xiao R, Liao X et al (2019) New insights into the formation and transformation of active species in nZVI/BC activated persulfate in alkaline solutions. Chem Eng J 359:1215–1223. https://doi.org/10.1016/j.cej.2018.11.056

Luo Z, Sheng K, Yin K et al (2022) Distinctive aging and inhibiting effects of microplastics between fresh and sulfidated nano-zero valent iron for various metal adsorption. Chem Eng J 431:133395. https://doi.org/10.1016/j.cej.2021.133395

Ma W, Sun T, Xu Y, Zheng S, Sun Y et al (2022a) In situ immobilization remediation, soil aggregate distribution, and microbial community composition in weakly alkaline Cd contaminated soils: a field study. Environ Pollut 292:118327. https://doi.org/10.1016/j.envpol.2021.118327

Ma Y, Cheng L, Zhang D, Zhang F, Zhou S, Ma Y, Guo J, Zhang Y, Xing B et al (2022b) Stabilization of Pb, Cd, and Zn in soil by modified-zeolite: mechanisms and evaluation of effectiveness. Sci Total Environ 814:152746. https://doi.org/10.1016/j.scitotenv.2021.152746

Puissant J, Jones B, Goodall T, Mang D, Blaud A, Gweon HS, Malik A, Jones DL, Clark IM, Hirsch PR, Griffiths R et al (2019) The pH optimum of soil exoenzymes adapt to long term changes in soil pH. Soil Biol Biochem 138:107601. https://doi.org/10.1016/j.soilbio.2019.107601

Rao Z, Zhu N, Wei X, Li F, Wu P, Dang Z, Cui B et al (2021) Efficient peroxydisulfate activation with nZVI/CuO@BC nanocomposite derived from wastes for degradation of tetrabromobisphenol A in alkaline environment. J Hazard Mater 417:126029. https://doi.org/10.1016/j.jhazmat.2021.126029

Shen B, Wang X, Zhang Y, Zhang M, Wang K, Xie P, Ji H et al (2020) The optimum pH and Eh for simultaneously minimizing bioavailable cadmium and arsenic contents in soils under the organic fertilizer application. Sci Total Environ 711:135229. https://doi.org/10.1016/j.scitotenv.2019.135229

Singh P, Pal P, Mondal P, Saravanan G, Nagababu P, Majumdar S, Labhsetwar N, Bhowmick S et al (2021) Kinetics and mechanism of arsenic removal using sulfide-modified nanoscale zerovalent iron. Chem Eng J 412:128667. https://doi.org/10.1016/j.cej.2021.128667

Song P, Ma W, Gao X, Ai S, Wang J, Liu W et al (2022) Remediation mechanism of Cu, Zn, As, Cd, and Pb contaminated soil by biochar-supported nanoscale zero-valent iron and its impact on soil enzyme activity. J Clean Prod 378:134510. https://doi.org/10.1016/j.jclepro.2022.134510

Tang J, Zhao B, Lyu H, Li D et al (2021) Development of a novel pyrite/biochar composite (BM-FeS_2@BC) by ball milling for aqueous Cr(VI) removal and its mechanisms. J Hazard Mater 413:125415. https://doi.org/10.1016/j.jhazmat.2021.125415

Wang J, Deng Z, Feng T, Fan J, Zhang WX et al (2021a) Nanoscale zero-valent iron (nZVI) encapsulated within tubular nitride carbon for highly selective and stable electrocatalytic denitrification. Chem Eng J 417:129160. https://doi.org/10.1016/j.cej.2021a.129160

Wang J, Wang P, Gu Y, Kopittke P, Zhao F, Wang P et al (2019) Iron–manganese (oxyhydro) oxides, rather than oxidation of sulfides, determine mobilization of Cd during soil drainage in paddy soil systems. Environ Sci Technol 53(5):2500–2508. https://doi.org/10.1021/acs.est.8b06863

Wang L, Chen H, Wu J, Huang L, Brookes PC, Mazza R, Xu J, Liu X et al (2021b) Effects of magnetic biochar-microbe composite on Cd remediation and microbial responses in paddy soil. J Hazard Mater 414:125494. https://doi.org/10.1016/j.jhazmat.2021.125494

Wang Y, Liang H, Li S, Zhang Z, Liao Y, Lu Y, Zhou G, Gao S, Nie J, Cao W et al (2022) Co-utilizing milk vetch, rice straw, and lime reduces the Cd accumulation of rice grain in two paddy soils in south China. Sci Total Environ 806:150622. https://doi.org/10.1016/j.scitotenv.2021.150622

Xiao M, Hong S, Shen X, Du Z, Yuan T et al (2023) In vivo cadmium-assisted dilute acid pretreatment of the phytoremediation sweet sorghum for enzymatic hydrolysis and cadmium enrichment. Environ Poll 324:121372. https://doi.org/10.1016/j.envpol.2023.121372

Xu H, Gao M, Hu X, Chen Y, Li Y, Xu X, Zhang R, Yang X, Tang C, Hu X et al (2021) A novel preparation of S-nZVI and its high efficient removal of Cr(VI) in aqueous solution. J Hazard Mater 416:125924. https://doi.org/10.1016/j.jhazmat.2021.125924

Xue W, Huang D, Zeng G, Wan J, Zhang C, Xu R, Cheng M, Deng R et al (2018) Nanoscale zero-valent iron coated with rhamnolipid as an effective stabilizer for immobilization of Cd and Pb in river sediments. J Hazard Mater 341:381–389. https://doi.org/10.1016/j.jhazmat.2017.06.028

Yang D, Yang S, Wang L, Xu J, Liu X et al (2021a) Performance of biochar-supported nanoscale zero-valent iron for cadmium and arsenic co-contaminated soil remediation: insights on availability, bioaccumulation and health risk. Environ Pollut 290:118054. https://doi.org/10.1016/j.envpol.2021.118054

Yang D, Yang S, Yuan H, Wang F, Wang H, Xu J, Liu X et al (2021b) Co-benefits of biochar-supported nanoscale zero-valent iron in simultaneously stabilizing soil heavy metals and reducing their bioaccessibility. J Hazard Mater 418:126292. https://doi.org/10.1016/j.jhazmat.2021b.126292

Yang T, Xu Y, Huang Q, Sun Y, Liang X, Wang L, Qin X, Zhao L et al (2021c) An efficient biochar synthesized by iron-zinc modified corn straw for simultaneously immobilization Cd in acidic and alkaline soils. Environ Pollut 291:118129. https://doi.org/10.1016/j.envpol.2021.118129

Yang Z, Guo W, Cheng Z, Wang G, Xian J, Yang Y, Liu L, Xu X et al (2022) Possibility of using combined compost–attapulgite for remediation of Cd contaminated soil. J Clean Prod 368:133216. https://doi.org/10.1016/j.jclepro.2022.133216

Yao, B., Wang, S., Xie, S., Li, G., Sun, G et al (2022) Optimal soil Eh, pH for simultaneous decrease of bioavailable Cd, As in co-contaminated paddy soil under water management strategies. Sci Total Environ 806:151342. https://doi.org/10.1016/j.scitotenv.2021.151342

Yuan Y, Wei X, Yin H, Zhu M, Luo H, Dang Z et al (2022) Synergistic removal of Cr(VI) by S-nZVI and organic acids: the enhanced electron selectivity and pH-dependent promotion mechanisms. J Hazard Mater 423:127240. https://doi.org/10.1016/j.jhazmat.2021.127240

Zhang L, He Y, Lin D, Yao Y, Song N, Wang F et al (2022a) Co-application of biochar and nitrogen fertilizer promotes rice performance, decreases cadmium availability, and shapes rhizosphere bacterial community in paddy soil. Environ Pollut 308:119624. https://doi.org/10.1016/j.envpol.2022.119624

Zhang X, Liu X, Peng Y, Wu X, Tan Y, Zeng Q, Song Z, Li M et al (2022b) Controllable shell corrosion of coated nanoscale zero valent iron induces long-term potentiation of its reactivity for uranium removal. Sep Purif Technol 287:120550. https://doi.org/10.1016/j.seppur.2022.120550

Zhu F, Wu Y, Liang Y, Li H, Liang W et al (2020) Degradation mechanism of norfloxacin in water using persulfate activated by BC@nZVI/Ni. Chem Eng J 389:124276. https://doi.org/10.1016/j.cej.2020.124276